Correlation of AFM and SFA Measurements Concerning the Stability of Supported Lipid Bilayers

Marcel Benz,* Thomas Gutsmann,† Nianhuan Chen,* Rafael Tadmor,‡ and Jacob Israelachvili*§
*Department of Chemical Engineering, †Department of Physics, and §Materials Research Laboratory, University of California, Santa Barbara, California 93106; and ‡Department of Chemical Engineering, Lamar University, Beaumont, Texas 77710

ABSTRACT Phospholipid bilayers were studied by means of atomic force microscopy (AFM) and a surface force apparatus (SFA). The stability of the supported bilayers was described by the amount of irregularities in the topography of the membrane by means of AFM and by the occurrence of hemifusion in the SFA, which is an indicator of defective bilayers. The bilayers, composed of lipids having the same headgroup but different chain lengths in the two leaflets, were prepared by Langmuir-Blodgett deposition and transferred at different surface pressures. The topography of the supported bilayers in aqueous solution, as imaged by AFM, revealed an increasing number of defects in the supported lipid membranes with decreased deposition pressure of the outer lipid layer. These defects, which appeared in the form of monolayer and bilayer (self-assembled) thick holes within the membrane, were energetically favorable over an evenly depleted bilayer. We found that the quantity of these defects (holes of ≤ 0.5 μm diameter and covering up to 30% of the surface area) correlated well with the stability of the bilayers as measured by SFA, a truly complementary instrument.

INTRODUCTION

The morphology of surfactants and especially phospholipid bilayers as imaged by atomic force microscopy is of immense current interest (Jass et al., 2000; Zasadzinski et al., 1991; Hansma and Hoh, 1994; Schwartz et al., 1992). One reason for this interest is that these lipids, together with proteins, are the major components of biological membranes. Various topographies in phospholipid bilayers, such as vacancies/holes (Schneider et al., 2000), protrusions (Santos et al., 1998), channels (Grandbois et al., 1998), and blisters (Rinia et al., 1999) have been imaged by AFM. A lot of attention has been given to the long-term stability and pH dependence of supported bilayers (Hui et al., 1995), which is of particular importance when they are used as intermediate or end products, e.g., as substrates for protein/polymer addition or as membrane coatings for biosensors (Kuhl et al., 1994). Likewise, the stability of supported bilayers above the chain melting temperature in the liquid crystalline state as well as below this temperature was studied with x-ray and differential scanning calorimetry (Nakano et al., 2000). Schneider et al. (2000) presented a methodology to analyze AFM force curves on lipid bilayers that correlated with topographical features in the AFM images. In that study surface contrasts were produced by phase-separated mixed monolayers of different lipids. Similar interests gave rise to the present study of phospholipid bilayer stability, with a focus on the influence of the lateral pressure (gel or liquid lipid phase) and the temperature during the lipid deposition.

The surface force apparatus (SFA) has been used frequently to measure both the forces between and stability of symmetrical and asymmetrical lipid bilayers (Marra and Israelachvili, 1985; Israelachvili and Marra, 1986). In these studies, molecular mechanisms associated with bilayer adhesion and ease of fusion were studied (Helm et al., 1989, 1992), where the latter is a direct indication of bilayer stability.

In this study the stabilities of supported phospholipid bilayers were investigated with two complementary instruments—AFM and SFA—and the results were correlated with each other. The topographical features in membranes described above (holes, protrusions, etc., that are different from the main uniform membrane) will be generally referred to as defects. All the defects we observed did not appear to change with time (up to 3 days), and may therefore represent the thermodynamically equilibrated distribution in the membranes. However, they may also be nonequilibrium structures that are slowly evolving with time. The bilayers were constructed from two uncharged zwitterionic double-chain phospholipids on mica: dipalmitoylphosphatidylethanolamine (DPPE) built the inner and dilauroylphosphatidylethanolamine (DLPE) the outer supported monolayer. The study of a DPPE/DLPE lipid bilayer has the following advantages: The two molecules have identical headgroups but differ by four CH_2 groups per chain, which is enough to dramatically change their phase state during compression. Although DPPE builds a very stable and rigid layer that remains in the solid phase over the entire range of lateral pressures studied (between 0 and 45 mN/m), DLPE shows a pronounced phase transition at ~35 mN/m at room temperature. In addition, DPPE has a high chain melting temperature or so-called phase transition temperature (T_c) of 63°C compared to DLPE (T_c = 30.5°C) and thus shows a very steep isotherm (vide infra) (Sández et al., 2002). This is due to the condensed, crystalline nature of DPPE, which makes the molecular area occupied by the lipid of the first monolayer (~41 Å^2) almost independent of the lateral pressure during a Langmuir deposition. Thus, the use of these two lipids allows the study of bilayers where

Submitted June 11, 2003, and accepted for publication September 24, 2003.
Address reprint requests to Jacob Israelachvili, E-mail: jacob@engineering.ucsb.edu.

0006-3495/04/02/870/10 $2.00

different deposition parameters such as temperature and lateral pressure allow control of the properties of the outer (DLPE) layer. Further, it is to our advantage that much data is already available for the two phospholipids. The pressure-area isotherms (Π vs. A) of DLPE have been well characterized by x-ray diffraction (Strzalka et al., 2000; Helm et al., 1991) and fluorescence microscopy (Helm and Möhwald, 1988; Ariga and Okahata, 1994). These studies have shown that the fluid-gel transition in DLPE is not sharp but involves a broad regime of coexisting fluid and ordered phases.

MATERIALS AND METHODS

Langmuir monolayer and bilayer deposition

The phospholipids DPPE and DLPE were obtained from Avanti Polar Lipids (Alabaster, AL). The lipids were dissolved in a chloroform/methanol (10:1) solution and spread on Millipore (Billerica, MA) filtered water pH = 6.0. Langmuir-Blodgett (LB) deposition is the method of choice for the controlled deposition of insoluble surfactants and lipids. The technique also offers a suitable way to assemble asymmetric bilayers with known surface coverage of inner and outer monolayers. Before each LB deposition at constant lateral pressure (dipping speed = 2.5 mm/min) an entire isotherm was recorded (lipid compression/expansion with 25 cm^2/min barrier speed) to fully evaporate the solvent. In our study, the lipids were LB deposited onto a supporting substrate of freshly cleaved mica discs (0.2-mm thick, 15-mm diameter). These discs were used for all the AFM analyses. Similarly, for all SFA measurements, the Langmuir deposition proceeded onto molecularly smooth mica sheets (2–3-μm thick) attached to cylindrical silica discs as commonly used in SFA experiments. The deposition of the stable DPPE first monolayer on mica was always done at 23°C, whereas DLPE was deposited below and above its chain melting point (30.5°C), at 23 and 33°C, respectively. The temperature in the trough solution was regulated with an external thermostat to within ~0.5°C. As is common for LB depositions on mica, the monolayers were deposited by pulling the substrate vertically up through the air-water interface, whereas bilayers were formed by passing the DPPE-coated substrate vertically down into the trough. Consequently, in the general case, where the bilayer is in a bathing solution, the substrates always carried the first monolayer of DPPE with its headgroups facing the negatively charged, hydrophilic mica surface, and the second monolayer of DLPE with its headgroups facing the aqueous subphase. For all measurements on bilayers, the subphase in the AFM or SFA chamber consisted of the trough water from the DLPE deposition. A sufficient concentration (above cmc) of lipids in the subphase is important so as not to deplete the lipid bilayer (Helm et al., 1989, 1992). In our case with trough water as the bathing solution the topography of the bilayers did not change if measured 1 h or up to 3 days after the bilayer deposition. A supported membrane, in the case of a deposited bilayer, was never removed from the aqueous solution during the transfer to the AFM or SFA chamber in order for the outer monolayer to remain stable. An exception to this rule was at the end of an SFA experiment where the liquid was slowly drained from the apparatus chamber and the surfaces allowed to dry. This procedure removed the outer DLPE monolayer and left the inner hydrophobic surface of the DPPE layer exposed, which allowed the thickness measurement of both lipid layers.

Atomic force microscopy

The bilayers were prepared and deposited on freshly cleaved mica discs (Muscovite Ruby Mica grade 1, S & J Trading Inc., New York, NY) as described above. For AFM imaging in liquid, a S-profile silicon rubber seal (Veeco/Digital Instruments, Santa Barbara, CA) was pressed onto the mica disc and both were transferred to the AFM. The images were taken in air or in trough water from the lipid deposition (deionized water at pH 6.0) with a MultiMode scanning probe microscope with a J-scanner (Veeco/Digital Instruments) and a modified head. The modification of the conventional MultiMode head was based on an exchange of the red laser diode with an infrared (IR)-laser diode to reduce interference effects. All images were taken in tapping mode with a commercial hydrophilic, silicon cantilever (NSC15, MikroMasch, Portland, OR). The scanning speed corresponded to a 0.5–1-Hz line frequency and the scanning size of all images shown was 5×5 μm. The lowest possible force for scanning was used in all experiments. Qualitative assessments of the defects in the AFM images were performed by the Nanoscope software. To determine the height differences we generated histograms using Nanoscope software, exported the data to Origin (Northampton, MA), and fitted the data with a multipeak Gaussian function. All AFM experiments were performed at room temperature at 23°C, however, due to heating by the laser of the AFM the actual temperature in the scanning area might have been higher.

Surface force apparatus

The surface force apparatus measures the force F between two cylindrically curved, molecularly smooth surfaces as a function of their separation D (Israelachvili and Adams, 1976, 1978; Israelachvili and McGuiggan, 1988). An optical multiple-beam interference technique is employed to measure the controlled separation between the two surfaces with an accuracy of a few Å. In addition, the optical method that produces a series of colored fringes, known as fringes of equal chromatic order (FECO) (Tadmor et al., 2003), allows the simultaneous monitoring of the surface shape, for instance the contact area. One of the surfaces is mounted on a spring with spring constant K, which was chosen to be fairly stiff (around 1000 N/m) to apply relatively high loads to compress the two surfaces. From the measured deflection ΔD of the spring, the force F between the surfaces can be determined from Hook's law,

$$\Delta F = K\Delta D. \tag{1}$$

The corresponding interaction energy per unit area E between two flat surfaces is simply related to the force F between the two curved surfaces by the Derjaguin approximation:

$$E = F/2\pi R, \tag{2}$$

where R is the radius of the curved surfaces (typically ~2 cm).

Under a large compressive force the curved surfaces flatten elastically, more specifically, the mica sheet supporting glue becomes compressed. This deformation can be accurately observed from the shape of the FECO fringes, which represent a cross-sectional view of the contact. Consequently, the contact radius a and the geometry around the contact position can be determined. In the case of flattened FECOs, the Derjaguin approximation (Eq. 2) no longer applies. In its place, the mean pressure between the compressed surfaces can be calculated directly using the measured contact area:

$$P_{\text{mean}} = F/\pi a^2. \tag{3}$$

For two nonadhering surfaces the flattening of the surfaces occurs only when an external force is applied. In this case the flattened contact radius a varies with the applied force F according to the well-known Hertz theory (Hertz, 1881; Horn et al., 1987):

$$a = (RF/Y)^{1/3}, \tag{4}$$

where Y is the elastic modulus of the materials. Due to the cross-cylindrical configuration of the curved substrates the maximal pressure P is at the center of the contact area. For a ''Herzian'' contact $P_{\text{max}} = 1.5\ P_{\text{mean}}$ and the pressure decreases monotonically to zero at the contact boundary. As

a consequence of this, two nonadhering surfaces diverge (bifurcate) smoothly at the edge of the contact zone.

The elastic deformation of adhering surfaces is treated by the Johnson-Kendall-Roberts (JKR) theory (Johnson et al., 1971). In contrast to the Hertz theory, the JKR theory predicts that two adhering surfaces diverge sharply at the edge of the contact zone. In addition, the JKR theory allows the determination of the adhesion energy W_0 from the adhesion or ''pull-off'' force F_0 needed to separate the adhering surfaces, which according to Chen et al. (1991) and Leckband et al. (1993) for perpendicular crossed cylinders is:

$$\gamma = (1/2)W_0 = F_0/3\pi R, \quad (5)$$

where the surface or interfacial energy γ is by definition half of the adhesion energy W_0.

The above equations were used to calculate the pressures and adhesion energies in all of the SFA experiments. Generally, these equations are valid for SFA and AFM experiments. An example of the explicit application of the above equations will be given later in the SFA result section.

RESULTS AND DISCUSSION

The Π-A isotherms for DPPE at 23°C, DLPE at 23°C, and DLPE at 33°C are illustrated in Fig. 1. The symbols for the phase states and phase changes are according to the characterization of Helm et al. (1987, 1991), where phospholipids were analyzed in the fluid, gel, and solid regions. Both of the phospholipids studied showed reversible isotherms. At 23°C DPPE (T_c = 63°C) shows a typical isotherm for monolayers in the solid, rigid state, where the lipid molecular area barely varies as the external surface pressure is increased. At 23°C DLPE (T_c = 30.5°C) shows a pronounced kink in the isotherm at Π ≈ 35 mN/m. As Π exceeds Π_c (cf. Fig. 1) the Π-A isotherm becomes nearly horizontal, corresponding to the main phase transition (first order) between the fluid and the ordered gel phase. As mentioned in the introduction, the two phases coexist in this regime (*II*). At 33°C DLPE is above its melting point and the isotherm remains in the more mobile fluid state over the entire lateral pressure range.

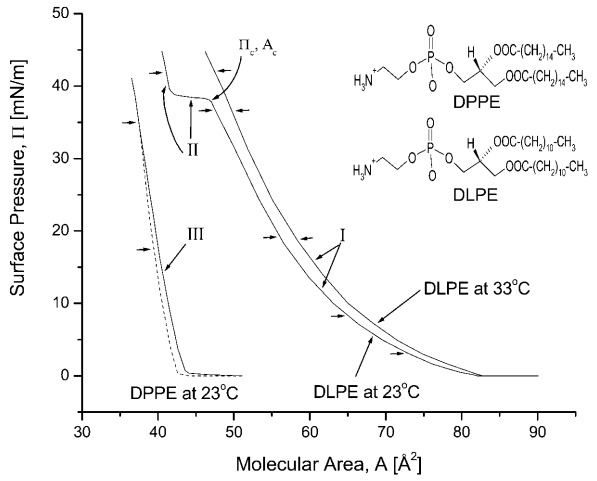

FIGURE 1 Measured isotherms (lateral surface pressure Π versus molecular surface area (A)) for monolayers of DPPE at 23°C and DLPE at 23°C and 33°C, respectively. The phase states of the lipids are also indicated in the isotherm (*I*, mobile fluid phase; *II*, coexisting fluid/ordered gel phase; and *III*, rigid solid phase) with the corresponding coordinate (Π_c, A_c) of pronounced change in the isotherm slope. The small horizontal arrows show the various lipid deposition pressures according to Table 1. All three lipids showed reversible isotherms. For clarity the reverse isotherm (*dashed line*) is only shown for DPPE. The chemical structure of the two phospholipids is shown in the upper right corner.

In the following, we focus on the deposition conditions of the outer DLPE monolayers. The inner DPPE monolayer was almost always deposited at the same temperature and high lateral pressure of Π ≈ 35 mN/m where it forms a stable and rigid monolayer in the solid phase. DLPE was deposited both above and below the phase transition temperature, T_c, as well as at different pressures. Table 1 gives an overview of the different monolayer and bilayer deposition conditions used in this study. The parameters lateral pressure (Π), consequently the lipid molecular area (A), and temperature (T) during the Langmuir deposition were varied. For the remainder of this article, these various phospholipid bilayers will be referred to according to the assigned deposition protocols of Table 1. The influence of the deposition condition was studied by AFM and SFA. All AFM and SFA measurements are performed at room temperature, 23°C, except for one SFA experiment with samples E-1 to E-3 performed at the DLPE deposition temperature of 33°C. Consequently, samples deposited above T_c were later measured below the lipids melting point.

Atomic force microscopy

In the first series of experiments DPPE monolayers were imaged with AFM in air (samples A-1 and A-2, data not shown). As expected, the surfaces of the DPPE layers are

TABLE 1 Deposition conditions of the LB deposited phospholipids

	First layer (lipid at 23°C)		Second layer (DLPE at T°C)	
Deposition	Lipid	Deposition pressure Π (mN/m)	T (°C)	Deposition pressure Π (mN/m)
A-1	DPPE	34	–	–
A-2		17		
B-1	DLPE	8	–	–
B-2		19		
B-3		37		
B-4		41		
C-1	DPPE	35		4
C-2		35		7
C-3	DPPE	34	23	19
C-4		34		37
C-5		34		42
D-1	DPPE	18	23	18
E-1	DPPE	36		19
E-2		36	33	37
E-3		36		42

very smooth and it can be assumed that the rigid lipids build a homogeneous layer over the mica substrate. The topography of DLPE monolayers was also examined. The lipids were LB deposited in the pressure range between 8 and 41 mN/m (samples B-1–B-4). Again, all described monolayers produced smooth and uniform films. As an example, the topography of DLPE sample B-1 (lowest lateral pressure of only 8 mN/m) is shown in Fig. 2 *B-1*. To confirm the existence of the uniform monolayer an area of 2 ± 2 μm was scratched into the monolayer with the cantilever in contact mode at a higher force. The subsequently image of a 5×5 μm area clearly showed the scratched region with a lipid monolayer height difference (data not shown).

As previously discussed, the inner lipid layer of a uniform supported bilayer is assumed to be totally covered by the outer monolayer and therefore never exposed to the water phase. However, this assumption becomes invalid if the outer layer contains discontinuities (defects). Thus, the effect of water exposure on a DPPE monolayer was examined next and shown in Fig. 2, *A-1a* and *A-1b*. Immediately after immersing the monolayer into water pronounced defects are observed. The heights of 2.6 ± 0.3 nm of the defects were determined from height histograms of the images. This value matches the length of the DPPE molecule (Marra and Israelachvili, 1985; Hui et al., 1995) determined in the SFA experiments. The same sample imaged after several hours of water exposure shows defects of roughly 4.0 ± 1.0 nm in height (deduced from respective height histograms), indicating that the initially desorbed DPPE lipids self-assemble to form a bilayer with the remaining supported lipids to overcome the unfavorable interaction of the hydrophobic hydrocarbon chain with water. The height of 4.0 nm is in the order of the thickness of the bilayer. The difference compared to the value determined in the SFA experiments (5.1 nm, vide infra) might be due to a relatively loose formation of the outer leaflet of the bilayer, allowing a deeper penetration of the cantilever tip into the membrane.

As the focus is shifted from monolayers to bilayers, all the AFM studies were performed in an aqueous environment. The outer leaflet of the first set of bilayers consisted of DLPE lipids that were deposited at room temperature below T_c (samples C-1–C-5). The inner DPPE layers were always deposited at the same pressure of 35 mN/m, but the outer DLPE layers were transferred at progressively higher pressures. Only bilayers C-4 (Fig. 3 *C-4*) and C-5 (not shown), transferred just below and above Π_c, showed smooth morphologies (0% defects, at least within the resolution limit of the AFM imaging of bilayers in a liquid; thus, defects on the molecular level cannot be excluded).

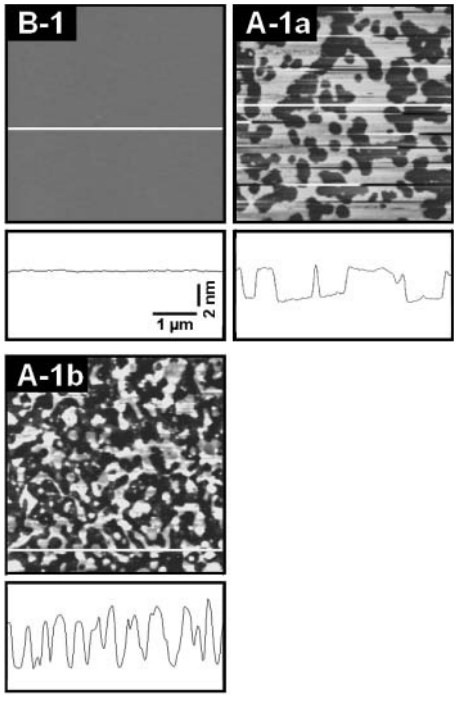

FIGURE 2 Monolayer imaged in air and in water. (*B-1*) DLPE monolayer deposited at a lateral pressure of 8 mN/m, imaged in air (sample B-1, refer to Table 1). (*A-1a*) DPPE monolayer deposited at a lateral pressure of 34 mN/m, imaged minutes after addition of deionized water (sample A-1). (*A-1b*) Same supported sample as in *A-1a* in deionized water but imaged several hours after the addition of water. All monolayers were prepared at room temperature (23°C) and were imaged in tapping mode at 23°C. The top row shows the height images and the bottom row the cross section indicated in the height image.

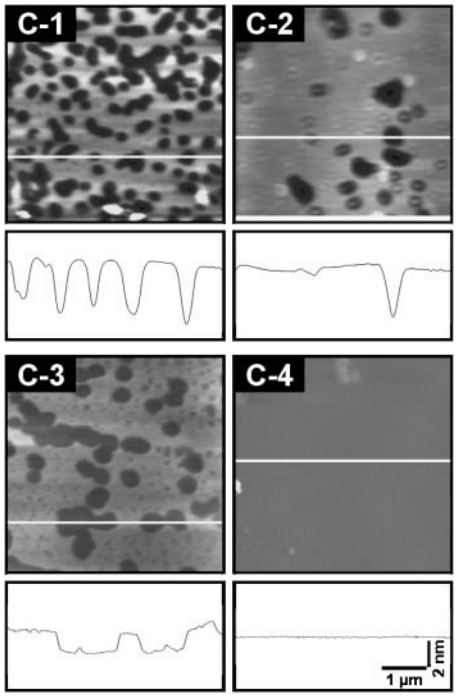

FIGURE 3 Influence of the lateral pressure at which the second DLPE monolayer was deposited (deposited at 23°C). In all four images the first monolayer consists of DPPE, which was deposited at a lateral pressure of 35 mN/m. The second monolayer of DLPE was deposited at (*C-1*) 4 mN/m (sample C-1); (*C-2*) 7 mN/m (sample C-2); (*C-3*) 19 mN/m (sample C-3); and (*C-4*) 37 mN/m (sample C-4). The top row shows the height images and the bottom row the cross section indicated in the height image.

However, if the transferring surface pressure of DLPE is reduced to 19 mN/m (Fig. 3 *C-3*) large defects of micrometer diameter in the form of holes are observed in the bilayers. The thickness of these defects is on the order of one monolayer, which results in the exposure of the hydrophobic DPPE hydrocarbon chains. Evidently, the outer monolayer with the lower lipid density does not simply form a uniformly thin layer but instead forms regions with fully developed bilayers and regions with monolayer holes, i.e., exposing the inner DPPE monolayer. The AFM images shown in Fig. 3, *C-1* and *C-2* (measured a few hours after the bilayer deposition) show the membrane with even lower DLPE deposition pressure (C-1 and C-2). The heights of the defects are 4.3 ± 0.3 nm and 4.1 ± 0.3 nm, respectively, which is on the order of a bilayer thickness, assuming lower values due to penetration of the tip into the bilayer (the profile of the smaller defects in Fig. 3 *C-2* is puzzling and is not discussed at this point). The diameter of the holes in C-1 and C-2 is smaller than in sample C-3, which strongly suggests that in equilibrium the desorbing DPPE lipids do not go into solution but anchor to the surrounding water-exposed hydrocarbon chains (DPPE lipids self-assemble with the remaining exposed monolayer as shown in Fig. 2 *A-1b*). In consequence, the magnitude of defects in sample C-2 is exactly the same as in C-3, namely, 18 ± 4%. The bilayer C-1 with the lowest DLPE surface pressure shows defects with the same diameter and height as sample C-2 but the number of holes per unit area is largely increased (30 ± 5%). This is in agreement with Bassereau and Pincet (1997) and Mou et al. (1995) who found that more defects of the same size appear when the second lipid layer is transferred at a lower surface pressure. The morphology of all samples remained unchanged when measured after 30 min and after several hours (data not shown), which indicates that the bilayers with their defects had fully equilibrated within <30 min of formation.

The bilayer D-1 (data not shown) was measured to confirm our choice of the inner DPPE lipid layer for building a rigid structure. The surface pattern as shown by AFM was alike for samples D-1 and C-3, which demonstrates that variations in the lateral surface pressure of the DPPE deposition has no influence on the bilayer stability due to the small dependency of the molecular lipid area on the surface pressure (see Fig. 1).

As mentioned before all AFM height and area measurements were calculated by means of histograms. An example of a height histogram of Fig. 3, *C-1* and *C-3*, is shown in Fig. 4. The histogram showed that in the case of sample C-3 predominantly monolayer deep holes were measured. For the bilayer C-1 mainly bilayer deep holes are indicated, however, monolayer deep holes cannot be excluded due to the wide distribution of the height measurements (*lower histogram* in Fig. 4). In addition, a schematic model was drawn of mono- and bilayer deep holes (Fig. 4) that resemble the molecular view of defects seen in Fig. 3, *C-1* and *C-3*.

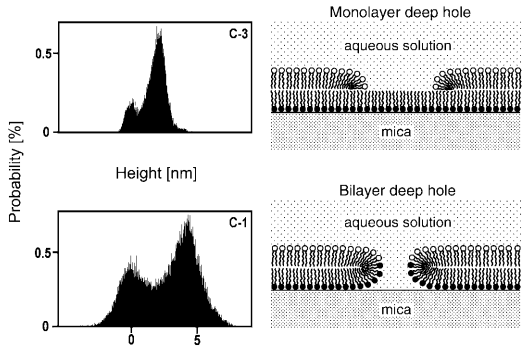

FIGURE 4 The left side of the figure shows the AFM histogram of monolayer and bilayer deep holes of samples C-3 and C-1, corresponding to Fig. 3, *C-3* and *C-1*, respectively. The diagram on the right side of the figure represents a schematic model of a monolayer and a bilayer deep hole, which are present in Fig. 3, *C-3* and *C-1*, respectively. The difference in the headgroup of the pictured lipids (●, ○) corresponds to the DPPE and DLPE lipids, respectively.

Finally, lipid bilayers were imaged where the DLPE layer was deposited at 33°C, i.e., above the lipid melting point T_c, and at various surface pressures (Fig. 5, *E-1–E-3*). Unlike bilayers C-4 and C-5 that were also transferred at high lateral pressures of DLPE and had smooth morphologies, E-2 and E-3 show signs of small defects. Due to the soft nature of these samples quantitative measurements of small instabilities were rather difficult. Generally, the defects had a width of ~60 nm and a height of 0.5 nm up to a monolayer in some cases. In addition, the amount of defects in E-3 was always the lowest and smaller than 1%. When DLPE was deposited in the fluid state ($T > T_c$) defects in the bilayer were created once the lipids cooled down to room temperature ($T < T_c$). It appears that the induced decrease of molecular area (refer to Fig. 1) during crystallization is sufficient to cause geometrical stresses/instabilities in the coverage of the bilayer.

Generally, AFM is very well suited for imaging topographies of supported lipid bilayers. It is also possible to determine the thickness of holes/defects, in particular to distinguish whether they span one monolayer of an entire bilayer in the membrane. However, the technique shows limitations when quantitative measurements of the height of defects are of interest, which have a diameter that is in the range of the diameter of the cantilever tip. The reason for this limitation is that the cantilever probe interacts with single or few molecules, which can lead to pushing down the lipids and/or the tip can penetrate into the sample (Schneider et al., 2000; Zasadzinski et al., 1991).

Surface force apparatus

For this study, rather stiff spring constants (1000–1500 N/m) were chosen to measure the normal forces to allow high loads on the compressing surfaces. Consequently, short-range interactions such as steric hydration and van der Waals forces were not the focus of this study. The reader is referred

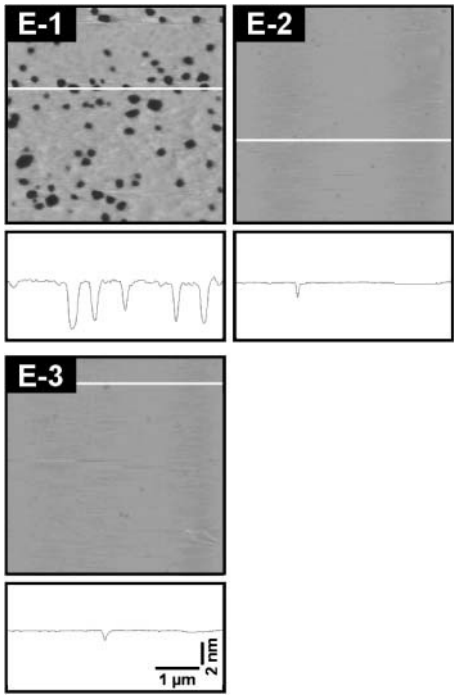

FIGURE 5 Influence of the lateral pressure at which the second DLPE monolayer was deposited (deposited at 33°C). In case of all three images the first monolayer consists of DPPE, which was deposited at a lateral pressure of 36 mN/m at room temperature (23°C). The second monolayer of DLPE was deposited at (*E-1*) 19 mN/m (sample E-1); (*E-2*) 37 mN/m (sample E-2); and (*E-3*) 42 mN/m (sample E-3). All bilayers were imaged in trough water from the LB deposition in tapping mode at room temperature (23°C). The top row shows the height images and the bottom row the cross section indicated in the height image.

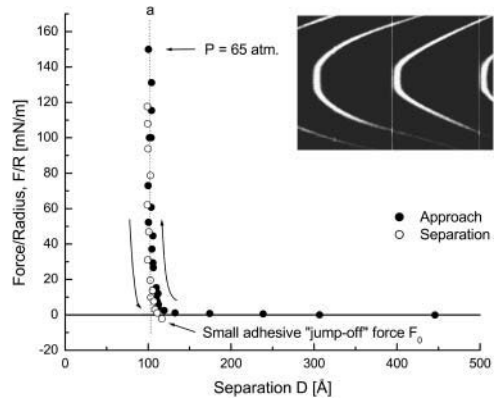

FIGURE 6 Repulsive force (*F*/*R*, force to radius) as a function of the distance between the two DPPE/DLPE bilayers assembled with deposition parameter C-5. $D = 0$ displays the mica-mica contact; thus, *a* corresponds to the hard wall, the thickness of two lipid bilayers. Only a small adhesion force is observed as the compressed bilayers (up to 65 atm) are separated from contact. The inset shows the FECO fringe pattern corresponding to C-5 bilayers that are compressed under load and show a flattened contact area.

to the work of Marra and Israelachvili (1985), Helm et al. (1992), and Israelachvili and Marra (1986) for more information on these bilayer interaction forces.

If lipid bilayers are compressed in the SFA and tested for the occurrence of hemifusion, one can gain information on the stability of the studied bilayers. Hemifusion describes the process of two bilayers fusing into one, also known as monolayer fusion (Chernomordik et al., 1987). Helm et al. (1989) found that the most important force leading to the direct fusion of bilayers is the hydrophobic interaction. In ''fully developed,'' ''unstressed,'' or ''saturated'' bilayers fusion could never be induced. However, depleting the bilayer by reducing the lipid concentration of the bathing medium below the critical micelle concentration caused hemifusion of the compressed bilayers. In our study, no hemifusion was forced by depleting the lipids (thinning of the absorbed bilayer by diluting the subphase), but the occurrence of hemifusion was used as an indicator of depleted/defective bilayers.

Fig. 6 shows a representative force-distance plot for bilayers deposited according to C-5, keeping in mind that the AFM measurements of these bilayers indicated no defect/instabilities at all (comparable to Fig. 3 *C-4*). With the SFA several different contact positions between the two surfaces were examined and multiple force-distance runs were measured at the same contact arrangement with maximum compression pressures, *P*, of over 100 atm. All the resulting plots were comparable and no hemifusion was ever observed. Instead, a hard wall at a thickness of two lipid bilayer and a small adhesion was always measured. These results support the conclusion of Helm et al. (1989) that when fully developed bilayers interact in water, their hydrophobic regions are effectively shielded from the aqueous phase, and consequently there is no hydrophobic contribution to the attraction between them. Thus, the occurrence of hemifusion is not to be expected if there are no defects (instabilities) in the bilayers. The average separation of the hard wall was measured to be 102 Å (averaged over several trials). After draining and drying the SFA chamber, an average surface separation of 52 Å was measured, which corresponds to two DPPE monolayers—one hydrophobic lipid layer remaining on each mica surface. Considering an interbilayer separation (water gap thickness) of 5–15 Å (Helm et al., 1992) a mean thickness of 25 and 19 ± 2 Å, is measured for fully developed inner DPPE and outer DLPE lipid layers, respectively.

A different SFA force-distance run was observed with C-3 bilayers where the DLPE layer was deposited at a lower lateral surface pressure. From the AFM images we already know that the outer DLPE layer contains fairly wide holes one monolayer deep. Thus, unlike the fully developed C-5 bilayers where no instabilities are present, C-3 samples seem to expose some of their inner hydrophobic regions. A representative SFA force-distance plot is shown in Fig. 7. The difference of the interbilayer forces is quite obvious. The average separation of the two bilayers once they are in contact is measured to be 102 Å, uniform over the area of

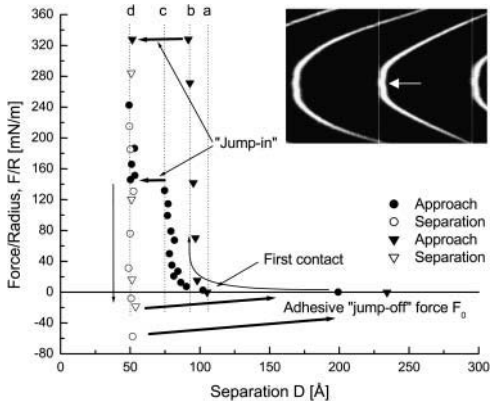

FIGURE 7 Force-distance plot of two DPPE/DLPE C-3 (*circles*) and E-3 (*triangles*) bilayers. $D = 0$ is the mica-mica contact. (*a*) Two uncompressed bilayers, contact at 102 Å; (*b*) two compressed E-3 bilayers just before hemifusion at 95 atm, 91-Å thickness; (*c*) two compressed C-3 bilayers just before hemifusion at 55 atm, 75-Å thickness; (*c*) two monolayers, 52-Å thickness corresponding to a hardwall of one bilayer (hemifused bilayers). A large ''jump-off'' force is measured due to the adhesive hemifused bilayer. The inset shows the FECO fringe pattern corresponding to C-3 bilayers just after hemifusion started, which is indicated by the abrupt step in the middle of the contact area.

contact and comparable with the previously measured value of 107 Å for the C-5 samples. However, the thickness of the bilayers decreases with further applied load, which is a reflection of the high compressibility of these bilayers. Then, at some point the applied load on the surfaces is large enough that the bilayers hemifuse, which is clearly seen by the spontaneous decrease of the separation distance from about 80 Å. The hemifused bilayer has an average thickness of 50 Å, which corresponds well to the above-measured DPPE-DPPE separation after draining the SFA chamber. This confirms that the initial 20–25 Å compressibility is due to the two depleted DLPE outer layers that are likely to be more disordered and/or fluid-like and therefore more compressible. The majority of the contact positions examined hemifused during the first compression. The fusion process always started at the center of the contact area and was complete within 30 s; this corresponds to a ''zipping rate'' of $\sim$1 μm/s.

Several characteristic numbers as introduced in the Materials and Methods section can be calculated by means of the measured data from the SFA force runs. The introduced equations are applied to the specific force-distance run with C-3 bilayers shown in Fig. 7. Surface separations were accurately measured as low as 5 Å. This corresponded to a measuring sensitivity in F of <0.5 μN ($K = 1100$ N/m, Eq. 1) and the sensitivity in measuring interfacial energies with the Derjaguin approximation ($R = 2.0$ cm, Eq. 2) of 4 μJm^{-2}. The mean pressure between the compressed surfaces can be calculated at any point. Just before the hemifusion the applied pressure P was 55 atm. ($F = 2.9$ mN, $a = 12.8$ μm, Eq. 3). The elastic modulus of the system can be calculated using the Hertz theory (Eq. 4). In the specific example the modulus was 27 GPa. Finally, one can calculate the adhesion energy, which in the example from Fig. 7 was 12.2 mJ/m^2 ($F_0 = 1.15$ mN, Eq. 5). Further calculations can be done that compare the adhesion energy with the bilayer thickness (Helm et al., 1992) or the exposed hydrophobic area. A purely hydrophobic hydrocarbon-water interface corresponds to an adhesion energy W of 100 mJ/m^2. Accordingly, the exposed hydrophobic area of bilayer C-3, which was measured as 18% (refer to Table 2) contributes to an adhesion energy of 18 mJ/m^2, which is very close to the experimentally measured value of 15 mJ/m^2.

The concept of hemifusion is understood as a progression where the outer lipid headgroups of opposite sides of the bilayers start to part laterally. This process exposes the hydrophobic hydrocarbon regions of both the outer and inner chains. Due to the long-range nature of the hydrophobic interaction (Israelachvili and Pashley, 1982, 1984; Pashley et al., 1985), the separation of the outer lipid layer is immediately followed by the attraction (''jump-in'') of the opposing hydrophobic regions. Thus, before hemifusion the initially unbroken bilayers showed a nonadhesive Hertzian shape, viz. rounded corners around the contact area that indicate a smooth nonadhesive divergence of the bilayers and maximal pressure in the center of the contact area where fusion eventually starts. Once hemifused, the shape of the contact area is governed by the JKR theory due to the adhesive hydrophobic interaction: the FECO fringes from the SFA's optical interference technique now show a sharp edge around the corner of the contact area within seconds after hemifusion starts. As shown in Fig. 7, hemifused bilayers show a much-increased adhesion (pull-off force) when the surfaces are separated compared to the weak adhesion of unfused bilayers. Two examples of FECO fringes of nonfused membranes and bilayers where the hemifusion just started are shown as insets in Figs. 6 and 7. Further examples of hemifusing fringe pattern were published by Helm et al. (1989; 1992).

A very similar force-distance run was observed with samples C-1 where the outer DLPE layer was transferred at $\Pi = 4$ mN/m. Every contact position measured showed hemifusion of the bilayers at comparatively low compressive loads. From the AFM images (Figs. 2 and 3) we know that monolayer thick defects reorient to expose holes of one bilayer thickness; thereby shielding the exposed DPPE lipids compared to the C-3 samples. Yet, it appears that despite this reordering of the defects, the instabilities in the bilayer are sufficiently pronounced so that hemifusion is reached at comparatively low applied pressure P. This is likely due to the strong depletion of the lipid bilayer. Furthermore, unlike in the previously studied samples, hemifusion starts at multiple positions generally closer to the edge of the contact position. The first fusion site is likely to be randomly located in the contact area because there is a high density of instabilities in bilayers with deposition C-3.

TABLE 2 Summary of the main results of the AFM and SFA analyses of supported lipid bilayers

	C-5	E-3	C-3	C-1
AFM				
Defected area	0%	<1%	18 ± 4%	30 ± 5%
Type of defect (height)	N.a.	≤ Monolayer	Monolayer	Bilayer
SFA				
Number of force runs	7	10	19	7
Hemifusion occurrence	0%	20%	70%	100%
F/R of 1st time hemifusion [mN/m]*	N.a.	~350	~250	~130
P of 1st time hemifusion [atm]*	N.a.	~120	~60	~20
Bilayer compressibility	~5%	10–15%	~20%	~20%
Separation just before hemifusion [Å]†	N.a.; hard wall at 102 ± 3	90 ± 3	79 ± 4	80 ± 3
Bilayer healing‡	N.a.	<5 h	~24 h	Several days
Adhesion energy W_0 [mJ/m^2]	~0.4	~5§	~15§	~21§
Location of fusion on contact	N.a.	Center	Center	Multiple positions

*Averaged load (force/radius) and pressure (P = F/A) that was required for the first hemifusion at a specific contact position.
†Surface separation just before the hemifusion occurs, each surface contains a lipid bilayer.
‡Required relaxation time after hemifusion to regain approximately three-fourths of the initial required fusion force.
§Adhesion energy of hemifused bilayers (n.a.: not applicable since fusion did not occur).

Next, lipid samples with deposition parameters E-3 were studied in the SFA. It is known from the AFM measurements that there are small defects in the bilayers despite the high deposition pressure Π of DLPE. Depending on the contact position and the number of times the surfaces were compressed and decompressed, a different force-distance curve was measured. Initially (first compression at a specific contact position), most measurements did not lead to hemifusion and the force-distance plot resembles the one with bilayers C-5 (Fig. 6). Later, on subsequent compressions at the same contact position, hemifusion was frequently detected. A force-distance profile where hemifusion occurred is also shown in Fig. 7. The main difference in the fusion behavior of the E-3 samples compared to that of C-3 samples was the smaller compressibility of the bilayer, a higher fusion force, and a smaller jump-off distance (adhesion force, F_0). The smaller adhesion values are consistent with all of the previous measurements. It can be concluded that bilayers with more defects require less force for fusion; however, once hemifused they show a higher adhesion as measured from the separation force F_0. The increased adhesion can be understood by the decreased strength of the outer, more depleted, DLPE lipid layer to restore a full bilayer. In the instances where the E-3 bilayers did not hemifuse at the highest loads applied (the maximum load was determined by the range of the electrical motor that drives the surfaces together and corresponded to a pressure of $P \approx 100$ atm), hemifusion could be forced by compressing the surfaces even more with the ''manual'' coarse micrometer drive. The difference between the various contact positions is probably due to the number and/or size of the bilayer defects per area, which can be slightly different for different regions (the contact position in a SFA experiment is ~30 μm in diameter). Helm et al. (1992) calculated a minimum diameter (d_{crit}) of a strongly depleted spot big enough to induce hemifusion. With their model, which included the contribution of the attractive hydrophobic forces versus the opposing surface rigidity forces, they calculated a value of $d_{crit} \approx 75$ nm. This would imply that samples of lipid bilayers E-3 are borderline cases for hemifusion, because the measured diameter of the defects in these samples (~60 nm) was close to d_{crit} as calculated above. The fact that several surface compressions were often necessary to induce hemifusion may be an indication that the bilayer is destabilized to some degree with each approach, and requires more time to totally regain its initial stability. This was a general observation in all the samples and could be quantified by measuring the necessary load to induce hemifusion as surfaces were compressed repeatedly at the same contact position. A reduced fusion force was commonly seen if no time was given for the bilayer to reorganize (''heal'') after a compression cycle. Accordingly, once hemifused bilayers are separated from contact they need a certain time to regain equilibrium where quantitatively reproducible force runs can be done. Lipid molecules in the fluid state readily exchange places with their neighbors within a monolayer (~10^7 times per second). This gives rise to a rapid lateral diffusion, with a diffusion coefficient (D) of ~10^{-8} cm^2 s^{-1} for an average lipid molecule (Alberts et al., 1983) (D is approximately four order lower in the gel phase; McKiernan et al., 2000). The time to regain equilibrium is expected to depend on the phase state of the lipid (the temperature) and the lateral and normal pressures Π and P on the bilayer. In the case of E-3 deposited bilayers subsequent force-distance profiles were measured with decreasing reequilibration (healing) times between fusions. Subsequently, we could compare the loads (F/R) required for hemifusion with the ''healing'' times between two runs. A load of 330 mN/m was measured for the first hemifusion at a specific contact position; subsequent measurement after 14 h required 262 mN/m, 5 h 245 mN/m, 30 min 244 mN/m, 15 min 216 mN/m, 5 min 160 mN/m, and 0 min 109 mN/m.

In the specific case of E-3 deposited membranes it appears that bilayers regain most of the stability within 30 min, although, the initial stability (compared to first-time fusion force) is not fully regained. However, quantitative measurements differed among different contact positions and thus contain a fair margin of error. Despite this fact, quantitative comparisons (averaged) between different bilayers were possible (vide infra). One of the reasons for the different healing kinetics of the same bilayer is the time that membranes remain in the hemifused state. Bilayers that remain for an increased period in the hemifused state experience a decrease in their subsequent stability after separation. As an example, two E-3 bilayers were kept in the fused state over night. After separation and reapproach they jumped into the hemifused state from an interbilayer distance of ~150 Å, i.e., well before the two surfaces were even in contact.

Finally, SFA measurements of the E-3 bilayers were performed at 33°C (above T_c of DLPE). Despite the phase change of the DLPE lipids from the coexisting fluid/gel phase to the liquid phase at higher temperature, no significant differences from the measurements at 23°C were observed.

Despite numerous compressions, fusion, and healings, the supported bilayers remained stable over the timeframe of the SFA experiments of more than 4 days. The duration of the hemifusion process was comparable for all the samples and generally occurred within 15–30 s over a contact diameter of ~30 μm (hemisfused area $\approx$ 700 μm^2). In the present study no significant differences in the fusion kinetics (the rate at which the hemifused region spread out) were seen despite the different phase states of the bilayers and measurements above and below T_c. This is in contrast to the reports by Helm et al. (1989; 1992), where more rigid lipids, gel, or solid phase, were found to have much slower kinetics (hours versus seconds) compared to fluid phase lipids.

CONCLUSIONS

This study compares measurements of the stability to fusion of supported phospholipid bilayers obtained from AFM and SFA. AFM images best describe the morphology of the bilayers that were transferred at different lateral surface pressures and temperatures of the outer lipid layer. A decreased outer lipid density leads to defects in the bilayers that form holes of a monolayer depth, and eventually self-assemble (''flip-flop'') to leave holes of one exposed bilayer depth as the deposition pressure Π of the outer lipid is further reduced. The increase of the size in the holes in bilayers with decreasing deposition pressure was also reported by Bassereau and Pincet (1997). However, their explanation of the origin of the bilayer deep holes was based on the lipid transfer ration; specifically by peeling off of the inner monolayer during the transfer of the second monolayer. Monolayer deep holes were thought not to be energetically stable, which is in strong contrast to our findings (as mentioned above). The reason that the formation of micrometer wide holes is energetically favorable in the supported bilayers over an evenly depleted membrane is unclear. A possible explanation was given by McKiernan et al. (2000) who speculated that the bilayer deep holes were caused by lipid dewetting of the mica surface.

SFA data on the other hand offers exceptional information on the stability (conditions for hemifusion) and thickness of bilayers, and especially of two interacting bilayers. In this respect, the stability measurements performed with the SFA could be well correlated with the results of the AFM images of single, isolated bilayers. Qualitative and quantitative comparisons between different bilayers were obtained and are summarized in Table 2. The following general conclusions with respect to bilayer healing (relaxation) are valid for all samples: 1), the activation force for fusion falls after each compression cycle; 2), bilayers hardly ever regain their initial stability (initial fusion force) within 24 hours; 3), prolonging the time that bilayers remain in the hemifused state decreases their subsequent stability after separation.

As AFM images show more defects/instabilities in the topography of the lipid bilayer, the force required for hemifusion as measured with the SFA steadily decreases. These stability characteristics are especially helpful when the supported membrane is intended for further applications, for example, in the basic research of membrane-mediated processes or when lipids are used as coatings for biosensors. Thus, the combination of AFM and SFA has proven to be very useful, as the two instruments are complementary in the way that the appearance of single defects in lipid bilayers, detected by the high spatial resolution of AFM, can be related to the averaged stability of the bilayer as measured by SFA. In addition, the surface force apparatus provides a technique to study the kinetics of lipid bilayer adhesion, fusion, and healing, which is of interest to those concerned with wound healing as an example.

Although free membrane bilayers behave differently compared to supported bilayers, the formation of holes in the membranes as discussed in this study may be relatable to the existence of pores in free bilayer membranes (Zahn and Brickmann, 2002; Taupin et al., 1975; Volkov et al., 1997). Similarly this study shows that defects/holes lead to hemifusion, which can be compared to membrane fusion through point defects in free bilayers as seen by Hui et al. (1981) and Fornes and Procopio (1995). Fusion of bilayers plays an important role in many cell-cell and cell-compartment interactions, e.g., in edocytosis and exocytosis. Thus, a mechanism reducing the energy barrier to induce membrane fusion as described in this article might be a process that also happens in biological systems.

This work was funded by the Swiss National Science Foundation, the National Science Foundation, through the Materials Research Science and Engineering Centers program (award no. DMR 9988640), the Materials Research Laboratory (MRL) program (award no. DMR00-80034), the

National Institutes of Health (award no. 8R01EB00380-09 and GM65354), the NASA/URETI on Bio Inspired Materials (award no. NCC-1-02037), and the Deutsche Forschungsgemeinschaft (project GU 568/2-1).

REFERENCES

Alberts, B., D. Bray, J. Lewis, M. Raff, K. Roberts, and J. D. Watson. 1983. Molecular Biology of the Cell. Garland Publishing, Inc. New York.

Ariga, K., and Y. Okahata. 1994. Hydration behavior of phospholipids Langmuir-Blodgett (LB) films deposited on a quartz-crystal microbalance depending on temperatures in water. *Langmuir*. 10:2272–2276.

Bassereau, P., and F. Pincet. 1997. Quantitative analysis of holes in supported bilayers providing the adsorption energy of surfactants on solid substrates. *Langmuir*. 13:7003–7007.

Chen, Y. L., C. Helm, and J. Israelachvili. 1991. Measurements of the elastic properties of surfactants and lipid monolayers. *Langmuir*. 7:2694–2699.

Chernomordik, L. V., G. B. Melikyan, and Y. A. Chizmadzhev. 1987. Biomembrane fusion—a new concept derived from model studies using 2 interacting planar lipid bilayers. *Biochim. Biophys. Acta*. 906:309–352.

Fornes, J. A., and J. Procopio. 1995. Density fluctuations in lipid monolayers and their possible relevance to the formation of conductive defects in bilayers. *Langmuir*. 11:3943–3947.

Grandbois, M., H. Clausen-Schaumann, and H. Gaub. 1998. Atomic force microscope imaging of phospholipid bilayer degradation by phospholipase A_2. *Biophys. J*. 74:2398–2404.

Hansma, H. G., and J. H. Hoh. 1994. Biomolecular imaging with the atomic force microscope. *Annu. Rev. Biophys. Biomol. Struct*. 23:115–139.

Helm, C. A., and H. Möhwald. 1988. Equilibrium and nonequilibrium features determining superlattices in phospholipid monolayers. *J. Phys. Chem*. 82:1262–1266.

Helm, C. A., H. Möhwald, K. Kjaer, and J. Als-Nielsen. 1987. Phospholipid monolayers between fluid and solid states. *Biophys. J*. 52: 381–390.

Helm, C. A., J. N. Israelachvili, and P. M. McGuiggan. 1989. Molecular mechanisms and forces involved in the adhesion and fusion of amphiphilic bilayers. *Science*. 246:919–922.

Helm, C. A., J. N. Israelachvili, and P. M. McGuiggan. 1992. Role of hydrophobic forces in bilayer adhesion and fusion. *Biochemistry*. 31:1794–1805.

Helm, C. A., P. Tippmann-Krayer, H. Möhwald, J. Als-Nielsen, and K. Kjaer. 1991. Phases of phosphatidyl ethanolamine monolayers studied by synchrotron x-ray scattering. *Biophys. J*. 60:1457–1476.

Hertz, H. 1881. J. Reine Angew. *Math*. 92:156–171.

Horn, R. G., J. N. Israelachvili, and F. Pribac. 1987. Measurement of the deformation and adhesion of solids in contact. *J. Colloid Interface Sci*. 115:480–492.

Hui, S. W., R. Viswanathan, J. A. Zasadzinski, and J. N. Israelachvili. 1995. The structure and stability of phospholipid bilayers by atomic force microscopy. *Biophys. J*. 68:171–178.

Hui, S. W., T. P. Steward, L. T. Boni, and P. L. Yeagle. 1981. Membrane-fusion through point-defects in bilayers. *Science*. 212:921–923.

Israelachvili, J. N., and G. E. Adams. 1976. Direct measurement of long-range forces between two mica surfaces in aqueous KNO_3 solutions. *Nature*. 262:774–776.

Israelachvili, J. N., and G. E. Adams. 1978. Measurement of forces between two mica surfaces in aqueous electrolyte solutions in the range of 0–100 nm. *J. Chem. Soc. Faraday Trans. I*. 74:975–1001.

Israelachvili, J., and J. Marra. 1986. Direct methods for measuring conformational water forces (hydration forces) between membrane and other surfaces. *Methods. Enzymol*. 127:353–360.

Israelachvili, J. N., and P. M. McGuiggan. 1988. Forces between surfaces in liquids. *Science*. 241:795–800.

Israelachvili, J. N., and R. M. Pashley. 1982. The hydrophobic interaction is long-range, decaying exponentially with distance. *Nature*. 300:341–342.

Israelachvili, J. N., and R. M. Pashley. 1984. Measurement of the hydrophobic interaction between 2 hydrophobic surfaces in aqueous-electrolyte solutions. *J. Coll. Int. Sci*. 98:500–514.

Jass, J., T. Tjärnhage, and G. Puu. 2000. From liposomes to supported, planar bilayer structures on hydrophilic and hydrophobic surfaces: an atomic force microscopy study. *Biophys. J*. 79:3153–3163.

Johnson, K. L., K. Kendall, and A. D. Roberts. 1971. Surface energy and contact of elastic solids. *Proc. R. Soc. London A*. 324:301–320.

Kuhl, T. L., D. E. Leckband, D. D. Lasic, and J. N. Israelachvili. 1994. Modulation of interaction forces between bilayers exposing short-chained ethylene oxide headgroups. *Biophys. J*. 66:1479–1488.

Leckband, D., C. Helm, and J. Israelachvili. 1993. Role of calcium in the adhesion and fusion of bilayers. *Biochemistry*. 32:1127–1140.

Marra, J., and J. Israelachvili. 1985. Direct measurements of forces between phosphatidylchlorine and phosphatidylethanolamine bilayers in aqueous electrolyte solutions. *Biochemistry*. 24:4608–4618.

McKiernan, A. E., T. V. Ratto, and M. L. Longo. 2000. Domain growth, shapes, and topology in cationic lipid bilayers on mica by fluorescence and atomic force microscopy. *Biophys. J*. 79:2605–2615.

Mou, J., J. Yang, and Z. Shao. 1995. Atomic force microscopy of cholera toxin B-oligomers bound to bilayers of biologically relevant lipids. *J. Mol. Biol*. 248:507–512.

Nakano, M., R. Inoue, M. Koda, T. Baba, H. Matsuaga, T. Natori, and T. Handa. 2000. Anomeric effects on the stability of bilayers of galactosylphytoceramides and on the interaction with phospholipids. *Langmuir*. 16:7156–7161.

Pashley, R. M., P. M. McGuiggan, B. W. Ninham, and D. F. Evans. 1985. Attractive forces between uncharged hydrophobic surfaces—direct measurements in aqueous solution. *Science*. 229:1088–1089.

Rinia, H. A., R. A. Demel, J. P. J. M. Van der Eerden, and B. de Kruijff. 1999. Blistering of Langmuir-Blodgett bilayers containing anionic phospholipids as observed by atomic force microscopy. *Biophys. J*. 77:1683–1693.

Sández, M. I., A. Suárez, and A. Gil. 2002. Surface pressure—area isotherm and fluorescent behavior of phospholipids containing labeled pyrene. *J. Coll. Int. Sci*. 250:128–133.

Santos, N. C., E. T. Ovanesyan, J. A. Zasadzinski, M. Prieto, and M. A. R. B. Castanho. 1998. Filipin-induced lesions in planar phospholipid bilayers imaged by atomic force microscopy. *Biophys. J*. 75:1869–1873.

Schneider, J., Y. F. Dufrene, W. R. Barger, and G. U. Lee. 2000. Atomic force microscope image contrast mechanisms on supported lipid bilayers. *Biophys. J*. 79:1107–1118.

Schwartz, D. K., J. Garnaes, R. Viswanathan, and J. A. N. Zasadzinski. 1992. Surface order and stability of Langmuir-Blodgett films. *Science*. 257:508–511.

Strzalka, J., X. Chen, C. C. Moser, P. L. Dutton, B. M. Ocko, and J. K. Blasie. 2000. X-ray scattering studies of maquette peptide monolayers. *Langmuir*. 16:10404–10418.

Tadmor, R., N. Chen, and J. N. Israelachvili. 2003. Thickness and refractive index measurements using multiple beam interference fringes (FECO). *J. Coll. Int. Sci*. 264:548–553.

Taupin, C., M. Dvolaitzky, and C. Sauterey. 1975. Osmotic pressure induced pores in phospholipid vesicles. *Biochemistry*. 14:4771–4775.

Volkov, A. G., S. Paula, and D. W. Deamer. 1997. Two mechanisms of permeation of small neutral molecules and hydrated ions across phospholipids bilayers. *Bioelectrochem. Bioenerg*. 42:153–160.

Zahn, D., and J. Brickmann. 2002. Molecular dynamics study of water pores in a phospholipid bilayer. *Chem. Phys. Lett*. 352:441–446.

Zasadzinski, J. A. N., C. A. Helm, M. L. Longo, A. L. Weisenhorn, S. A. C. Gould, and P. K. Hansma. 1991. Atomic force microscopy of hydrated phosphatidylethanolamine bilayers. *Biophys. J*. 59:755–760.